

High-order-harmonic generation of a doped semiconductor

Tengfei Huang,¹ Xiaosong Zhu,^{1,*} Liang Li,¹ Xi Liu,¹ Pengfei Lan,^{1,†} and Peixiang Lu^{1,2,‡}

¹*School of Physics and Wuhan National Laboratory for Optoelectronics, Huazhong University of Science and Technology, Wuhan 430074, China*

²*Laboratory of Optical Information Technology, Wuhan Institute of Technology, Wuhan 430205, China*

(Received 27 September 2017; published 31 October 2017)

We investigate the high-order-harmonic generation (HHG) in doped semiconductors. The HHG is simulated with the single-electron time-dependent Schrödinger equation. The results show that the high-order harmonics in the second plateau generated from the doped semiconductors is about one to three orders of magnitude higher than those from the undoped semiconductor. The results are explained based on the analysis of the energy-band structure and the time-dependent population imaging. Our paper indicates that doping can effectively control the HHG in semiconductors.

DOI: [10.1103/PhysRevA.96.043425](https://doi.org/10.1103/PhysRevA.96.043425)

I. INTRODUCTION

With the fast development of laser technology, the interaction between intense laser pulses and matters has been studied extensively over the past several decades and revealed many interesting phenomena [1–3]. One of the most interesting phenomena is high-order-harmonic generation (HHG) [4,5], because it promises many important and unprecedented applications like generating coherent ultrafast extreme violet radiations [1,6–8] and probing the ultrafast dynamics of atomic, molecular, and solid systems [9–13].

Recently, high-order harmonics emitted from the bulk solids were detected [14]. Compared with the gas, the solid has periodic structure and high density [15,16]. Therefore, it has potential to produce more efficient HHG than the gas [17]. By analyzing the spectrum of the solid HHG, it is possible to study the structures of solid materials [17–20]. The solid HHG can also provide a new path to investigate the attosecond electron dynamics in solid materials [21] and to reconstruct the energy-band structures of solid crystals [22].

Recent works have shown that the solid HHG has two-plateau structure [23–26]. The intensity of the second plateau is about five orders of magnitude lower than that of the primary plateau [24]. The one-band model [27] and multibands model [28–31] are used to explain the mechanism behind HHG. It is considered that the two-plateau structure is attributed to the multibands structure of the solid [28,29]. Wu *et al.* [25] suggest that the interband current between the valence band and the first conducting band contributes the primary plateau of the high-order-harmonic spectrum, and the interband current between the valence band and the second to the third conducting bands contributes the second plateau. On the other hand, the electron-hole recollision model in wave-vector k space is proposed to explain the mechanism of HHG in solids [17,26,30,31]. It is suggested that the first plateau arises from electron-hole recollision, while the higher plateaus arise from dynamic Bloch oscillations.

Nowadays, in energy-band engineering, doping is widely used to improve the physical, e.g., electrical, magnetic, and optical, characteristics of objects through changing the energy-band structures of the target [32]. This indicates that the characteristics of HHG in solids can be controlled by doping [33]. In this paper, we investigate HHG in the doped semiconductors and discuss the influence of doping on HHG. The results show that the energy bands are changed by doping and the intensity of the second plateau of HHG is improved by about one to three orders of magnitude compared with that of the undoped semiconductor. This result is analyzed based on the picture of energy bands and the time-dependent population imaging.

II. THEORETICAL MODEL

In our paper, we investigate the laser-crystal interaction and HHG in the doped and undoped semiconductor by solving the time-dependent Schrödinger equation (TDSE). The laser field is polarized along the \vec{x} axis. In the length gauge, the time-dependent Hamiltonian is written as

$$\hat{H} = \hat{H}_0 + xE(t) \quad (1)$$

where $\hat{H}_0 = \hat{p}^2/2 + v(x)$. Atomic units are used in this paper unless otherwise stated. $v(x)$ is the periodic potential of the lattice. In this paper, the undoped semiconductor is modeled by Mathieu-type potential [34] $v(x) = -v_0[1 + \cos(2\pi x/a_0)]$, with $v_0 = 0.37$ a.u. and the lattice constant $a_0 = 8$ a.u. The Mathieu-type potential has been widely used to simulate the optical lattice [35,36] and solid HHG [25,37,38].

For the doped semiconductor, we discuss the situation that the dopant replaces the atom of the undoped semiconductor periodically. We assume that the dopant will not change the lattice constant. The potential based on Mathieu-type potential is written as

$$v = \begin{cases} -v_0[1 + \cos(2\pi x/a_0)] & a \leq x \leq b \quad \text{or} \quad c \leq x \leq d, \\ -v_1[1 + \cos(2\pi x/a_0)] & b < x < c \end{cases} \quad (2)$$

The potentials of the doped (the blue dashed line) and undoped (the red solid line) semiconductor in a repetitive unit are shown in Fig. 1. The potential parameter of the dopant between b and c is $v_1 = 0.52$ a.u. One can see five atoms in

*zhuxiaosong@hust.edu.cn

†pengfeilan@mail.hust.edu.cn

‡lupeixiang@mail.hust.edu.cn

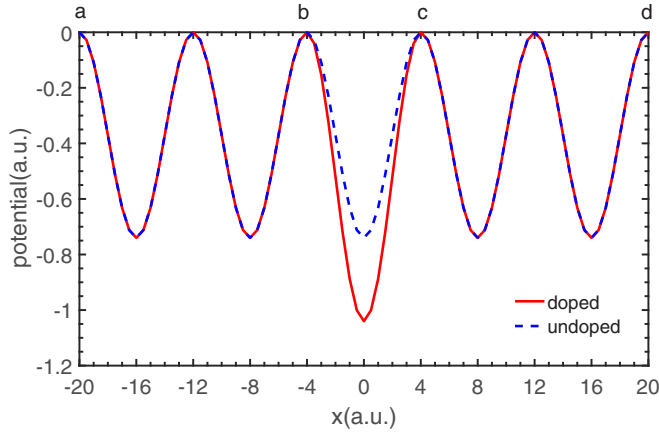


FIG. 1. The blue dashed line shows the potential of the one-dimensional (1D) undoped semiconductor. The red solid line shows the potential of the 1D doped semiconductor.

the region $[a, d]$. Between b and c , the potential parameter of the origin atom v_0 is replaced by that of the dopant atom v_1 . So the doping rate is 0.2.

To obtain the energy bands of the doped and undoped semiconductors, we solve the eigenvalue equation of \hat{H}_0 ,

$$\hat{H}_0 \varphi_n(x) = E_n \varphi_n(x), \quad (3)$$

where n is the eigenstate number and $\varphi_n(x)$ is the eigenstate wave function. To solve the eigenvalue equation, we diagonalize \hat{H}_0 on a coordinate grid [39]. With the finite-difference method, the operator \hat{H}_0 is represented by an $N \times N$ matrix \mathbf{H} , where N is the number of the grid points. The nonzero elements of the matrix \mathbf{H} are given by

$$\begin{aligned} \mathbf{H}_{i,i} &= \frac{1}{(dx)^2} + V_i, \\ \mathbf{H}_{i,i+1} &= -\frac{1}{2(dx)^2}, \\ \mathbf{H}_{i+1,i} &= \mathbf{H}_{i,i+1}, \end{aligned} \quad (4)$$

where the grid spacing dx is 0.25 a.u. and V_i is the i th element of the one-dimensional (1D) grid of $v(x)$. The results of both doped and undoped semiconductors are calculated in the real space within the region $[0, 4000]$ a.u. (500 lattice periods).

Figure 2 shows the energy-band structure of the doped and undoped semiconductors. The red circles and the black points correspond to the doped semiconductor and the undoped semiconductor, respectively. Each energy band of the undoped semiconductor can be distinguished clearly. The valance band (VB) and conducting bands (CB1, CB2, and CB3) correspond to the state numbers 501-1000, 1001-1500, 1501-2000, and 2001-2500. The energy gap between VB and CB1 is labeled as $e1$ and the energy gap between CB1 and CB2 is labeled as $e2$. It is shown in Fig. 2(b) that the band gaps $e1$ and $e2$ of the doped semiconductor are narrower than those of the undoped semiconductor.

Doping changes the periodicity of the semiconductor. Therefore, compared with the undoped semiconductor, the energy bands of the doped semiconductor are split into small bands and the small energy bands corresponding to state

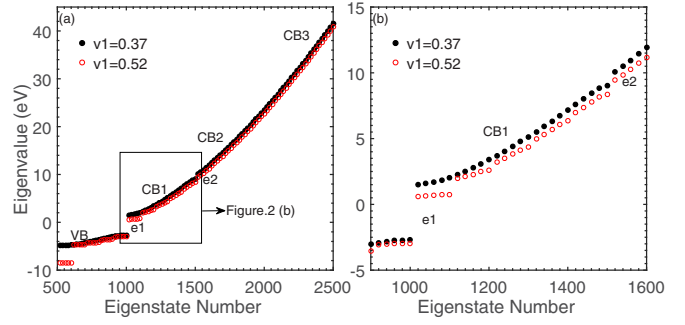


FIG. 2. (a) The energy-band structures of the doped and undoped semiconductors. The black points show the eigenvalue of the undoped semiconductor, while the red circles show the eigenvalue of the doped semiconductor. We choose one point every 20 points. (b) The band-structure region that includes the gaps $e1$ and $e2$.

number 1-100, 501-600, and 1001-1100 locate away from other energy bands. As a result, the energy gaps $e1$ and $e2$ become much narrower in the doped semiconductor.

To obtain the time-dependent wave function $\psi(t)$, we solve the TDSE using the second-order split-operator method:

$$\begin{aligned} \psi(t + dt) &= \exp\left(-\frac{idt\hat{T}}{2}\right) \exp(-idt\hat{V}) \\ &\quad \times \exp\left(-\frac{idt\hat{T}}{2}\right) \psi(t) + O(dt^3) \end{aligned} \quad (5)$$

where $\hat{T} = \hat{p}^2/2$ and $\hat{V} = v(x) + xE(t)$. The number of the time points is 10000. In Eq. (4), commutation errors give rise to the third-order term in dt . Equation (4) is solved by the spectral method [40]. We solve the first and the third term on the right-hand side in momentum space by the fast Fourier-transform algorithm. The second term is multiplied directly in position space. In this paper, we adopt a sine-squared envelope for the driving laser pulses with the total duration of eight optical cycles (t_c). The wavelength of the driven laser is $3.2 \mu\text{m}$ and the intensity is $8.087 \times 10^{11} \text{ W/cm}^2$. We choose the eigenstate populated at the top of the valence band as the initial state [25,37]. To overcome the unphysical reflections of the wave function $\psi(t)$ at the edges of the grid spacing, we use a $\cos^{1/3}$ absorbing boundary. The width of the absorbing boundary is kL , where $k = 0.0833$ is the scale and $L = 4000$ a.u. is the length of the real space we used. We find that the k is small enough to ensure the results are stabilized. Since the lowest band is very flat and deeply bound, it plays a negligible role in the HHG dynamics.

With the time-dependent wave function $\psi(t)$, the laser-induced current can be obtained as

$$j(t) = -\langle \psi(t) | \hat{p} | \psi(t) \rangle. \quad (6)$$

We multiply $j(t)$ by a Hanning window [25]. The harmonic spectrum is obtained by calculating the Fourier transform of the laser-induced current:

$$H(\omega) \propto |j(t) e^{i\omega t} dt|^2. \quad (7)$$

To better analyze the HHG in the doped and undoped semiconductors, the time-dependent population imaging (TDPI) is

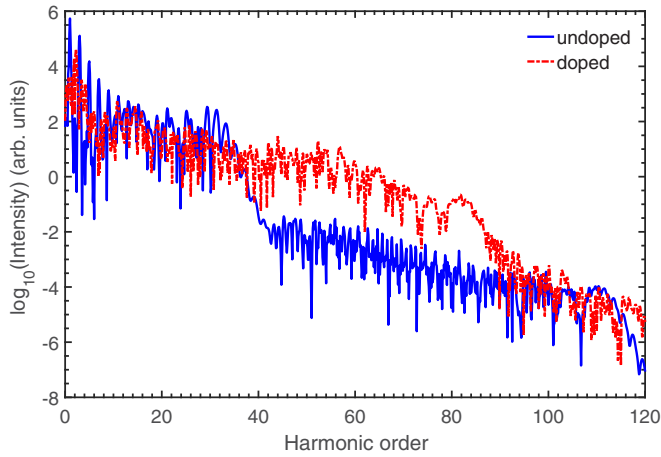


FIG. 3. The blue line shows the HHG spectrum of the undoped semiconductor. The red dash-dotted line shows the HHG spectrum of the doped semiconductor.

also calculated [39]. To obtain the TDPI, the instantaneous population $C_n(t)$ on each eigenstate is calculated by the modulus square of the time-dependent projection of $\psi(t)$ on φ_n as

$$|C_n(t)|^2 = \langle \varphi_n | \psi_n(t) \rangle^2. \quad (8)$$

The corresponding eigenvalue of φ_n is E_n . $|C_n(t)|^2$ can be understood as the time-dependent probability of electrons occupying on the eigenenergy E_n . Then the TDPI picture is obtained by plotting $|C_n(t)|^2$ as a function of time t and eigenenergy E_n .

III. RESULTS AND DISCUSSION

Figure 3 shows the HHG spectrum of the doped (blue solid line) and undoped (red dash-dotted line) semiconductors. The HHG spectrum of the undoped semiconductor shows a two-plateau structure. The first plateau starts at the 18th order and has a cutoff at the 32nd order. The second plateau starts at the

40th order and has a cutoff at the 112nd order. For the HHG spectrum of the doped semiconductor, the intensities of the high-order harmonics between the 10th and the 32nd orders are lower than those of the undoped semiconductor, while the intensities of the high-order harmonics between the 40th and the 80th orders are about two orders of magnitude higher than those of the undoped semiconductor. The second plateau is dramatically enhanced by the doping.

To understand the mechanism of the enhancement of the second plateau intuitively, we show the TDPI picture in Fig. 4. Figure 4(a) shows the electron populations in the energy bands of the undoped semiconductor. They are driven forth and back in each energy band by the external laser field. The oscillations of electron populations in the energy bands correspond to the laser-driving Bloch oscillations of electrons in reciprocal space. Figure 4(b) shows the electron populations in the energy bands of the doped semiconductor. Besides the oscillations of electron populations, one can also see the reflection of electron populations at the border of the energy bands, i.e., at the border of the Brillouin zone in Fig. 4(b). This is because the energy bands of the doped semiconductor are separated into small bands. As the doping rate is 0.2, the Brillouin zone of the doped semiconductor becomes 0.2 times of the undoped semiconductor. Therefore it is easier for electrons to oscillate to the border of the Brillouin zone of the doped semiconductor. And at the border of the Brillouin zone, the electrons can be reflected in the same band or much more easily tunnel to higher bands [41]. So the electron populations in CB2 and CB3 of the doped semiconductor are higher than those of the undoped semiconductor.

The phenomenon mentioned above can also be explained by the band structure of the doped semiconductor. When the laser field interacts with the semiconductor, the electrons in the VB begin to oscillate in the same band and have the possibility to tunnel to energy band CB1 through the band gap e_1 . We label it as process 1. After they populate on CB1, there are two possible paths. On the one hand, some of them can oscillate to the border of the Brillouin zone and tunnel to higher-energy bands CB2 and CB3 through a narrow band gap e_2 . Then these electrons in CB2 and CB3 can transfer to VB and radiate

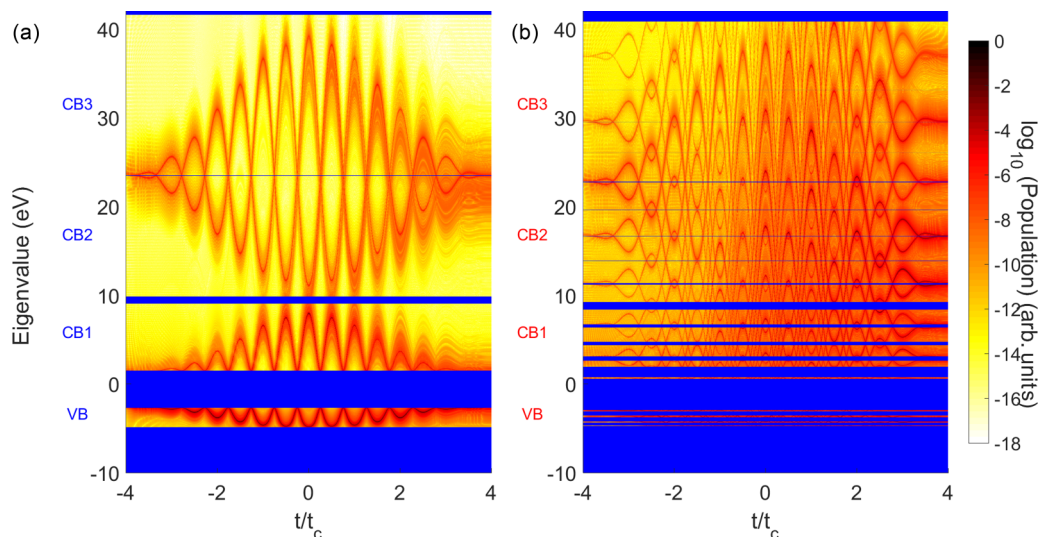


FIG. 4. (a) The TDPI picture of the undoped semiconductor model. (b) The TDPI picture of the doped semiconductor model. Blue areas are band gaps.

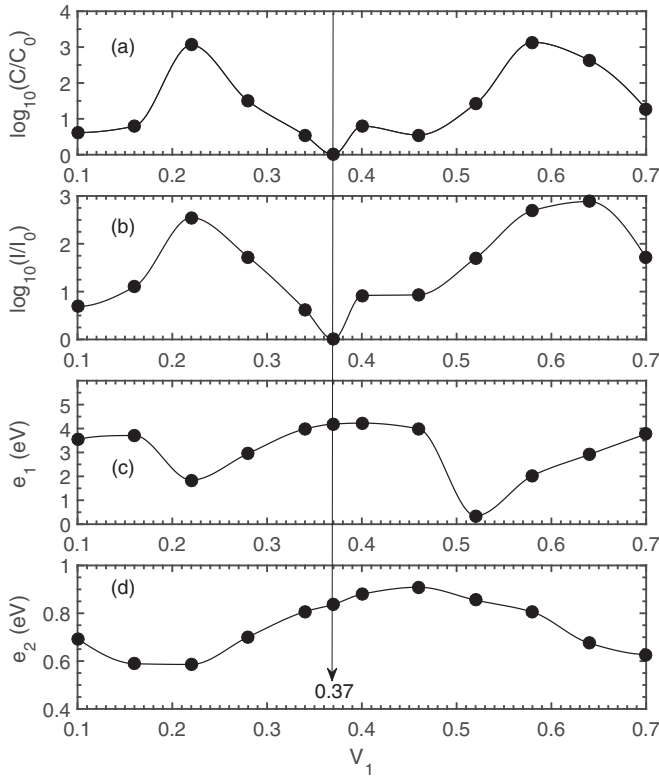


FIG. 5. (a) The comparison between the total population of CB2 and CB3 in the doped semiconductors with that of the undoped semiconductors. (b) The comparison of average intensity of the second plateau (between 40th and 80th orders) between the doped and undoped semiconductors. (c) The band gap e_1 between VB and CB1 of different doped semiconductors. (d) The band gap e_2 between CB2 and CB3 of different doped semiconductors.

high-order harmonics in the second plateau. We label this as process 2. On the other hand, some of the electrons in CB1 can transfer back to VB and radiate high-order harmonics in the first plateau. In Fig. 4(a), only a small portion of electrons of the undoped semiconductor can arrive at the top of CB1 (i.e., the border of the Brillouin zone), so process 1 and process 2 are weak. Thus the electron populations in CB2 and CB3 are small and the intensity of the second plateau is low. On the other hand, in Fig. 4(b), because the energy bands become smaller, most of the electrons can populate on the top of the small energy bands and tunnel to higher-energy bands. Additionally, it is shown in Fig. 2(b) that doping makes the band gaps e_1 and e_2 of the doped semiconductor narrower than those of the undoped semiconductor. Therefore, process 1 and process 2 are strengthened. Consequently, the electron populations in CB2 and CB3 of the doped semiconductor are larger. And the second plateau of the doped semiconductor is about two orders of magnitude higher than that of the undoped semiconductor. On the other hand, the smaller Brillouin zone and the narrower band gap e_1 can strength the populations in CB1, while the narrower band gap e_2 can make more populations in CB1 transfer to CB2, resulting in less transitions from CB1 to VB. So the intensity of the first plateau is about one order of magnitude lower than that of the undoped semiconductor.

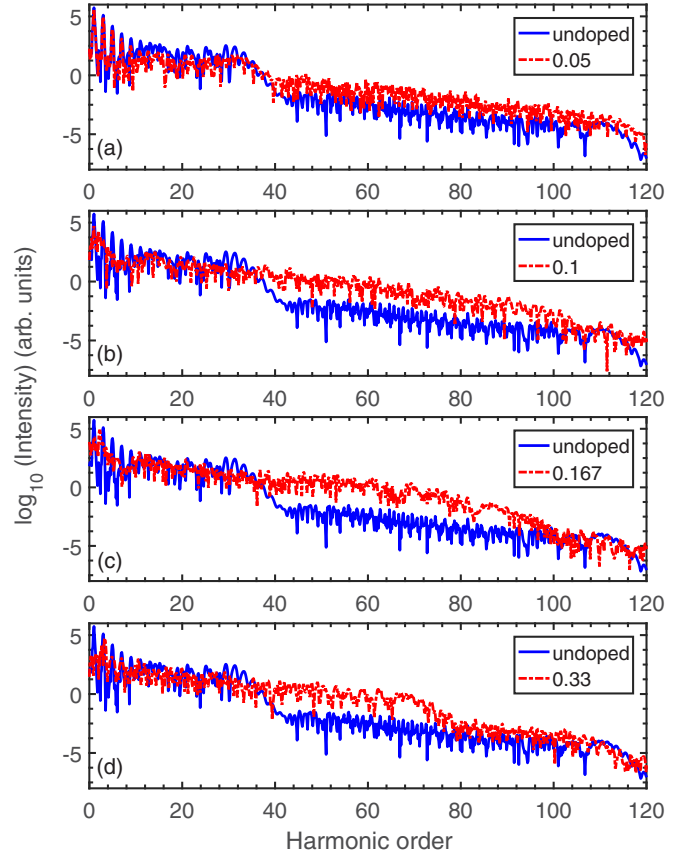


FIG. 6. The blue lines in each figure show the HHG spectrum of the undoped semiconductor. The red dash-dotted lines show the HHG spectrum of the doped semiconductors under different doping rates 0.05, 0.1, 0.167, and 0.33 in Figs. 6(a)–6(d). $v_1 = 0.52$ a.u.

To further investigate the effect of doping, we compare the populations on CB2 to CB3 of the doped semiconductors with different values of v_1 . The results are shown in Fig. 5. In Fig. 5(a), C is the total electron population of the energy bands CB2 to CB3 in the doped semiconductor, and C_0 is the population of the energy bands CB2 and CB3 in the undoped semiconductor. Figure 5(b) shows the comparison between the average intensities in the second plateau (between 40th and 80th orders) of the doped and undoped semiconductors. I is the average intensity of the high-order-harmonics spectrum of the doped semiconductors and I_0 is the average intensity of the undoped semiconductor. Compared with the undoped semiconductor ($v_1 = 0.37$), the average intensities of high-order harmonics of the doped semiconductors are all improved. It is also shown that the curves in Figs. 5(a) and 5(b) have similar variation tendency. They both have maximums around $v_1 = 0.22$ and minimums around $v_1 = 0.37$. Figure 5(c) shows the band gaps e_1 between VB and CB1 at different values of v_1 . Figure 5(d) shows the band gaps e_2 between CB2 and CB3 at different values of v_1 . The minimums of e_1 and e_2 around $v_1 = 0.22$ in Figs. 5(c) and 5(d) correspond to the maximums of populations and intensities in Figs. 5(a) and 5(b), while the maximums of e_1 and e_2 around $v_1 = 0.37$ correspond to the minimums of populations and intensities.

Figure 5 shows that with the decreasing band gaps e_1 and e_2 the possibilities of electrons tunneling to higher-energy bands become larger. Then the electron populations in the energy bands CB2 to CB3 and the intensity of the second plateau of the doped semiconductor high-order harmonics will be increased. The populations in CB2 to CB3 are primarily controlled by the band gap e_1 . Meanwhile, they can also be modulated by the band gap e_2 . Therefore one can control the species of dopants to control the semiconductor HHG, especially the second plateau.

We also investigate the HHG of the doped semiconductors under different doping rates at $v_1 = 0.52$ a.u. They are compared with that of the undoped semiconductor in Fig. 6. It is shown in Figs. 6(a) and 6(b) that the intensities of the high-order harmonics of the doped semiconductors between the 10th and the 32nd orders are about half those of the undoped semiconductor, while the intensity of the second plateau increases rapidly as the doping rate rises from 0 to 0.1. In Figs. 6(c) and 6(d), as the doping rate is larger than 0.1, the intensities of the high-order harmonics of the doped semiconductors between the 40th and the 70th orders are about one to two orders of magnitude higher than those of the undoped semiconductor.

IV. CONCLUSION

We simulate the HHG in the doped and undoped semiconductors based on a 1D single-electron model in periodic potentials. The results indicate that the HHG in the semiconductors can be effectively controlled by doping. Both TDPI and energy-band pictures are used to analyze the mechanism. Doping changes the energy-band structure of the semiconductors and makes the Brillouin zone and band gaps e_1 and e_2 narrower than before. The small Brillouin zone and narrow band gaps e_1 and e_2 strengthen the electron populations in CB2 to CB3, and improve the intensity of the second plateau of the high-order harmonics. Our paper indicates that one can control the HHG of the semiconductor by controlling the species of dopants and the doping rate.

ACKNOWLEDGMENT

This paper was supported by the National Natural Science Foundation of China under Grants No. 11234004, No. 11404123, No. 11574101, No. 11422435, and No. 11627809.

-
- [1] F. Krausz and M. Ivanov, *Rev. Mod. Phys.* **81**, 163 (2009).
- [2] P. B. Corkum and F. Krausz, *Nat. Phys.* **3**, 381 (2007).
- [3] Z. Wang, K. Liu, P. Lan, and P. Lu, *Phys. Rev. A* **91**, 043419 (2015); *J. Phys. B* **48**, 015601 (2015).
- [4] J. L. Krause, K. J. Schafer, and K. C. Kulander, *Phys. Rev. Lett.* **68**, 3535 (1992).
- [5] K. J. Schafer, B. Yang, L. F. DiMauro, and K. C. Kulander, *Phys. Rev. Lett.* **70**, 1599 (1993).
- [6] P. M. Paul, E. S. Toma, P. Breger, G. Mullot, F. Augé, P. Balcou, H. G. Muller, and P. Agostini, *Science* **292**, 1689 (2001).
- [7] M. Hentschel, R. Kienberger, C. Spielmann, G. A. Reider, N. Milosevic, T. Brabec, P. Corkum, U. Heinzmann, M. Drescher, and F. Krausz, *Nature (London)* **414**, 509 (2001).
- [8] F. Wang, W. Liu, L. He, L. Li, B. Wang, X. Zhu, P. Lan, and P. Lu, *Phys. Rev. A* **96**, 033407 (2017).
- [9] M. Uiberacker, T. Uphues, M. Schultze, A. J. Verhoef, V. Yakovlev, M. F. Kling, J. Rauschenberger, N. M. Kabachnik, H. Schröder, M. Lezius *et al.*, *Nature (London)* **446**, 627 (2007).
- [10] A. Schiffrin, T. Paasch-Colberg, N. Karpowicz, V. Apalkov, D. Gerster, S. Mühlbrandt, M. Korbman, J. Reichert, M. Schultze, S. Holzner *et al.*, *Nature (London)* **493**, 70 (2012).
- [11] S. R. Leone, C. W. McCurdy, J. Burgdörfer, L. S. Cederbaum, Z. Chang, N. Dudovich, J. Feist, C. H. Greene, M. Ivanov, R. Kienberger *et al.*, *Nat. Photonics* **8**, 162 (2014).
- [12] P. Lan *et al.*, *Phys. Rev. Lett.* **119**, 033201 (2017).
- [13] D. Wang, X. Zhu, X. Liu, L. Li, X. Zhang, P. Lan, and P. Lu, *Opt. Express* **25**, 23502 (2017).
- [14] S. Ghimire, A. D. DiChiara, E. Sistrunk, P. Agostini, L. F. DiMauro, and D. A. Reis, *Nat. Phys.* **7**, 138 (2010).
- [15] S. Ghimire, A. D. DiChiara, E. Sistrunk, G. Ndabashimiye, U. B. Szafruga, A. Mohammad, P. Agostini, L. F. DiMauro, and D. A. Reis, *Phys. Rev. A* **85**, 043836 (2012).
- [16] T. T. Luu, M. Garg, S. Yu. Kruchinin, A. Moulet, M. Th. Hassan, and E. Goulielmakis, *Nature (London)* **521**, 498 (2015).
- [17] G. Vampa, T. J. Hammond, N. Thiré, B. E. Schmidt, F. Légaré, C. R. McDonald, T. Brabec, and P. B. Corkum, *Nature (London)* **522**, 462 (2015).
- [18] C. Yu, X. Zhang, S. Jiang, X. Cao, G. Yuan, T. Wu, L. Bai, and R. Lu, *Phys. Rev. A* **94**, 013846 (2016).
- [19] S. Jiang, C. Yu, G. Yuan, T. Wu, Z. Wang, and R. Lu, *J. Phys.: Condens. Matter* **29**, 275702 (2017).
- [20] A. F. Kemper, B. Moritz, J. K. Freericks, and T. P. Devereaux, *New J. Phys.* **15**, 023003 (2013).
- [21] M. Schultze, K. Ramasesha, C. D. Pemmaraju, S. A. Sato, D. Whitmore, A. Gandman, J. S. Prell, L. J. Borja, D. Prendergast, K. Yabana, D. M. Neumark, and S. R. Leone, *Science* **346**, 1348 (2014).
- [22] G. Vampa, T. J. Hammond, N. Thiré, B. E. Schmidt, F. Légaré, C. R. McDonald, T. Brabec, D. D. Klug, and P. B. Corkum, *Phys. Rev. Lett.* **115**, 193603 (2015).
- [23] G. Ndabashimiye, S. Ghimire, M. Wu, D. A. Browne, K. J. Schafer, M. B. Gaarde, and D. A. Reis, *Nature (London)* **534**, 520 (2016).
- [24] M. Wu, D. A. Browne, K. J. Schafer, and M. B. Gaarde, *Phys. Rev. A* **94**, 063403 (2016).
- [25] M. Wu, S. Ghimire, D. A. Reis, K. J. Schafer, and M. B. Gaarde, *Phys. Rev. A* **91**, 043839 (2015).
- [26] T.-Y. Du and X.-B. Bian, *Opt. Express* **25**, 151 (2017).
- [27] K. A. Pronin, A. D. Bandrauk, and A. A. Ovchinnikov, *Phys. Rev. B* **50**, 3473(R) (1994).
- [28] P. G. Hawkins, M. Y. Ivanov, and V. S. Yakovlev, *Phys. Rev. A* **91**, 013405 (2015).
- [29] P. G. Hawkins and M. Y. Ivanov, *Phys. Rev. A* **87**, 063842 (2013).

- [30] G. Vampa, C. R. McDonald, G. Orlando, D. D. Klug, P. B. Corkum, and T. Brabec, *Phys. Rev. Lett.* **113**, 073901 (2014).
- [31] C. R. McDonald, G. Vampa, P. B. Corkum, and T. Brabec, *Phys. Rev. A* **92**, 033845 (2015).
- [32] J. D. Bryan and D. R. Gamelin, in *Progress in Inorganic Chemistry*, edited by K. D. Karlin (Wiley, New York, 2005), Vol. 54; H. Long, L. Bao, A. A. Habeeb, and P. Lu, *Opt. Quantum Electron.* **49**, 345 (2017).
- [33] J. D. Cox, A. Marini, and F. J. de Abajo, *Nat. Commun.* **8**, 14380 (2017).
- [34] J. C. Slater, *Phys. Rev.* **87**, 807 (1952).
- [35] B. M. Breid, D. Witthaut, and H. J. Korsch, *New J. Phys.* **8**, 110 (2006).
- [36] R. Chang, S. Potnis, R. Ramos, C. Zhuang, M. Hallaji, A. Hayat, F. Duque-Gomez, J. E. Sipe, and A. M. Steinberg, *Phys. Rev. Lett.* **112**, 170404 (2014).
- [37] Z. Guan, X.-X. Zhou, and X.-B. Bian, *Phys. Rev. A* **93**, 033852 (2016).
- [38] T.-Y. Du, Z. Guan, X.-X. Zhou, and X.-B. Bian, *Phys. Rev. A* **94**, 023419 (2016).
- [39] X. Liu, X. Zhu, P. Lan, X. Zhang, D. Wang, Q. Zhang, and P. Lu, *Phys. Rev. A* **95**, 063419 (2017).
- [40] M. D. Feit, J. A. Fleck, Jr., and A. Steiger, *J. Comput. Phys.* **47**, 412 (1982).
- [41] J.-B. Li, X. Zhang, S.-J. Yue, H.-M. Wu, B.-T. Hu, and H.-C. Du, *Opt. Express* **25**, 18603 (2017).